Single-crystal study on the heavy-fermion antiferromagnet UZn_{12}

A.P. Gonçalves[1,*], P. Estrela[2], A. de Visser[2], E.B. Lopes[1], I. Catarino[3], G. Bonfait[3], M. Godinho[4], M. Almeida[1], D. Gnida[5], D. Kaczorowski[5]

[1] Departamento de Química, Instituto Tecnológico e Nuclear, P-2686-953 Sacavém, Portugal.

[2] Van der Waals - Zeeman Institute, University of Amsterdam, Valckenierstraat 65, NL-1018 XE Amsterdam, The Netherlands.

[3] Departamento de Física, Universidade Nova de Lisboa

[4] Departamento de Física, Faculdade de Ciências, Universidade de Lisboa, Campo Grande ed. C1, P-1749-016 Lisboa, Portugal.

[5] Institute of Low temperature and Structure Research, Polish Academy of Sciences, P.O.Box 1410, 50-950 Wroclaw, Poland

Short title: heavy-fermion antiferromagnet UZn_{12}

PACS: 71.27.+a, 72.10.Fk, 75.50.Ee

Keywords: UZn_{12}, Heavy fermions, Intermetallics, Uranium compounds

* **Corresponding author:**
Dr. António Pereira Gonçalves
Departamento de Química,
Instituto Tecnológico e Nuclear,
P-2686-953 Sacavém
PORTUGAL
Tel: (+351)-21-9946182
Fax: (+351)-21-9941455
E-mail: apg@itn1.itn.pt

Abstract

Millimetre size UZn_{12} single crystals were grown by the High Temperature Solution Growth method using zinc as solvent. Single crystal x-ray diffraction data confirm that this compound crystallizes in the hexagonal high temperature form of $SmZn_{12}$ (S.G. P6/mmm) and points to a $U_{1.01(1)}Zn_{11.7(1)}$ stoichiometry for the crystals, with ~4% of the U atoms being located at the 2*c* site due to the partial substitution of 4*h* Zn pairs. UZn_{12} orders antiferromagnetically at $T_N = 5.0(2)$ K, the magnetization and resistivity measurements suggesting that the magnetic moments are confined within the *a*-*b* plane. The Sommerfeld coefficient, derived from the paramagnetic region by the standard method, is $\gamma_p \approx 200$ mJ/(mol K^2), which definitely classifies UZn_{12} as a moderate heavy-fermion system. The heavy-fermion character of UZn_{12} is also manifested in the overall shape of temperature-dependent electrical resistivity that is dominated by a single-ion Kondo effect at high temperatures and coherent Kondo scattering at low temperatures. The paramagnetic magetoresistivity isotherms can be fairly well superimposed onto each other using the Schlottmann's scaling for the single-ion Kondo model, as expected for a Kondo system.

1. Introduction

Uranium-, cerium- and ytterbium-based intermetallic compounds continue attracting much attention due to wide spectrum in their unusual physical properties [1,2]. Most of them belong to a class of strongly correlated electron systems, which exhibit at low temperatures enhanced magnitudes of the linear specific-heat coefficient, $\gamma(0)$, and the Pauli magnetic susceptibility, $\chi(0)$, both characteristics being proportional to a large effective mass, m*, at the Fermi level. A number of these so-called heavy-fermion systems order magnetically at low temperatures, usually with an antiferromagnetic arrangement of the magnetic moments [2].

Studies of the binary uranium-zinc phase diagram established the existence of two intermetallic compounds, U_2Zn_{17} and UZn_{12} [3]. U_2Zn_{17} was reported to crystallize in two distinct structure types, the rhombohedral Th_2Zn_{17}-type structure (space group R-3m) [4], stable at low temperatures, and the hexagonal Th_2Ni_{17}-type structure (space group $P6_3/mmc$) [4], stable above 724(3)ºC [3]. The U_2Zn_{17} polymorphic form crystallizing in the Th_2Zn_{17}-type structure has been deeply studied: the temperature dependence of the magnetic susceptibility, measured on polycrystalline samples, displays a broad maximum around 16 K, followed by a drop below 9.8 K, which was attributed to an antiferromagnetic ordering of the uranium moments [5]; more detailed studies on U_2Zn_{17} single crystals revealed a sharp cusp in the magnetic susceptibility, thus confirming the antiferromagnetic ordering below T_N = 9.8 K, and moreover indicated a sizeable magnetic anisotropy both in the antiferromagnetic and paramagnetic regions [6]. Above T_N, the specific heat over temperature ratio, C/T, attains a large value of 535 mJ/(mol K^2) [5], that manifests heavy-fermion character of the electronic ground state.

X-ray structural studies on small single crystals of UZn_{12} have shown that this compound is isostructural with the high-temperature form of $SmZn_{12}$ that crystallises in the hexagonal

structure with the P6/mmm space group [7]. However, the structure is disordered, leading to stoichiometries deficient in zinc, which is also corroborated by microprobe analysis that indicated single crystals with compositions $UZn_{(10.4\text{-}11.0)\pm0.1}$ [7]. Phase diagram studies confirm this picture, pointing to a composition range from $UZn_{9.4}$ to $UZn_{11.5}$ [3]. Specific heat measurements, performed on polycrystalline samples, revealed a heavy-fermion behaviour, with a $\gamma(0)$ term of 850-900 mJ/(mol K^2) [8,9]. The paramagnetic Curie temperature and the effective magnetic moment, derived from the Curie-Weiss fitting of the magnetic susceptibility data, were -83.15 K and 2.89 μ_B/U-atom, respectively. Neither magnetic nor superconducting phase transitions down to 0.4 K were observed [8,9].

The present work reports the growth of UZn_{12} single crystals and their comprehensive characterisation by means of X-ray diffraction, magnetisation, specific heat, resistivity and magnetoresistance measurements. These results are supplemented by muon spin relaxation spectroscopy, carried out on polycrystalline samples from the same batch.

2. Experimental

Single crystals with typical dimensions 1.5x1.5x0.2 mm^3 were prepared by the high temperature solution growth method, using zinc as solvent. The constituents, with a starting ratio between the uranium and zinc of 1:50, were put in a molybdenum ampoule that was sealed under argon atmosphere. This ampoule was placed in an evacuated quartz tube and heated up to 750ºC, held at this temperature for 4 hours and then cooled to 650ºC with a speed of 1ºC/min. At this last temperature the excess of liquid zinc was removed from the crystals by turning the ampoule upside down.

A small single-crystalline piece (0.1x0.1x0.1 mm^3), suitable for structural characterization, was extracted from a larger platelet. The crystal was glued on the top of a glass fiber, and

mounted on a goniometer head. The X-ray diffraction data were collected using a four-circle diffractometer (Enraf-Nonius CAD-4) with graphite-monochromatized MoKα radiation (λ = 0.71069 Å). The lattice parameters were obtained by the least-squares refinement of the 2θ values of 25 intense and well-centred reflections, taken from various regions of the reciprocal space.

The X-ray data were recorded at room temperature in a ω-2θ scan mode (Δω = 0.80 + 0.35•tgθ). Three reflections were monitored as intensity and orientation standards at 360 minutes intervals during data collection; no variation larger than 4% was observed. The intensities of the 3715 measured reflections (with $3^o \leq 2\theta \leq 90^o$) were corrected for absorption by an empirical method based on Ψ scans [10], as well as for Lorentz and polarization effects. The reflections were averaged, resulting in 756 independent intensities, from which 619 were considered ($I > 3\sigma(I)$).

The crystal structure was refined using the program UPALS [11]. The diffraction data were compatible with a hexagonal system, space group P6/mmm and hence the UZn_{12}-type structure was assumed [7]. The extinction and scale factors, nine anisotropic temperature factors, eight position parameters (*x*, *y* and *z* for the *12o* site, *x* for the *6j* and *6k* positions and *z* for the *2e*, *4h* and *6i* sites) and seven occupation factors were refined. Crystallographic and experimental data of the structural determination are listed in Table 1.

Magnetization measurements were performed on oriented single crystals (mass ~3 mg) in the 2-350 K temperature range and in external magnetic fields up to 5.5 T using a SQUID magnetometer (Quantum Design MPMS-5). The electrical resistivity was measured in the range 0.4-300 K with the current flowing along the crystallographic *a*-axis in zero magnetic field and in magnetic fields up to 9 T applied along and perpendicular to the c-axis. For these studies a single crystal of dimensions 1.0 x 0.27 x 0.13 mm^3 was used, and a conventional

four-probe method with an ac-resistance bridge was applied (implemented in a Quantum Design PPMS platform). Heat capacity measurements were performed on a single crystalline sample (mass ~5 mg) in the temperature interval 2-70 K in zero magnetic field, and in the range 2-17 K in fields up to 10 T applied perpendicular to the c-axis, using a relaxation method (with an Oxford Instruments Maglab system).

Muon spin relaxation (μSR) experiments were carried out on a polycrystalline sample taken from the same batch as the single crystals. Zero field spectra were recorded in the temperature range 2-10 K at the GPS (general-purpose spectrometer) facility of the Paul Scherrer Institute (Switzerland).

3. Results and discussion

3.1. Crystal structure

The refinement of the lattice parameters yielded the values of a = 8.9448(9) Å and c = 8.8984(8) Å, i.e. slightly smaller than those reported in the literature (a = 8.950(1) Å and c = 8.902(2) Å) [7]. The structure refinement procedure converged to R = 0.047 and R_W = 0.057, and confirmed the hexagonal high-temperature form of $SmZn_{12}$-type structure. The refined atomic positions, site occupancies, and thermal displacement factors are presented in Table 2.

The unit cell of UZn_{12} is illustrated in figure 1. The uranium atoms are mainly located in the 1*a* and 2*d* crystallographic positions, yet about 4% of uranium atoms were also found at the 2*c* position due to partial substitution of the 4*h* zinc pairs. The refinement gives the composition $U_{1.01(1)}Zn_{11.7(1)}$ in which the zinc content is higher than that previously reported for this compound [7], yielding a stoichiometry much closer to the 1:12 ideal one.

The coordination numbers (CN) for the inequivalent crystallographic sites and the relevant interatomic distances (up to 3.60 Å) are listed in Table 3. The uranium nearest-neighbour coordination polyedra are shown in figure 2. A coordination number of 20 is observed for all the uranium positions. However, for the U_3 atoms at the 2*c* sites (with 4% occupation) CN should be considered as equal to 18, as a result of the partial substitution for the 4*h* zinc pairs (see figure 2c). This structural feature is particularly well reflected in very short interatomic distances from U_3 to the Zn_6 atoms (1.293 Å), which are much smaller than the sum of the respective metallic radii (1.39 Å for zinc and 1.53 Å for uranium, for a coordination number of 12 [12]). All the other distances of the U atoms to the nearest neighbour Zn atoms are much larger than that sum, hence pointing to reduced f-d hybridization effects. In turn, the shortest uranium-uranium distances are 4.449 Å (2*d*-2*c* positions), and 5.164 Å (1*a*-2*c* and 2*d*-2*d* positions), i.e. they are well above the Hill limit (~3.4 Å) for effective f-f hybridization. These two structural features of UZn_{12} should promote formation of appreciable uranium magnetic moments which might order at low temperatures.

In spite of uranium environments similar to those in the U_2Zn_{17} compound, with only zinc atoms being the nearest neighbours of uranium atoms, and large uranium-uranium distances being well above the Hill limit, UZn_{12} was claimed to exhibit no superconductivity or magnetic order down to 0.4 K [8,9]

3.2. Magnetic behavior

The temperature variations of the magnetic susceptibility measured with the magnetic field applied along the *a*- and *c*-axis of single-crystalline UZn_{12} are shown in figure 3. An antiferromagnetic-type anomaly is observed at 5.0(2) K for both directions, yet it is much less

pronounced for B || *c*-axis, hence suggesting that the magnetic moments are confined within the *a*-*b* plane . Some magnetic anisotropy is also apparent in the paramagnetic state. Above 10 K, the inverse magnetic susceptibility follows the Curie-Weiss law with the effective magnetic moments μ^{a}_{eff} = 2.15(4) μ_B/U-atom and μ^{c}_{eff} = 2.28(2) μ_B/U-atom, for the magnetic field applied along the *a*- and *c*-axis, respectively, and the paramagnetic Curie temperatures θ^{a} = -35.6(4) K and θ^{c} = -40.1(3) K, for the *a*- and *c*-axis, respectively. The anisotropy manifests in both the μ_{eff} and θ values, yet its magnitude (measured roughly by the difference $\Delta\theta = \theta^{a} - \theta^{c}$) is much lower than usually observed for uranium compounds [13]. As shown in figure 4, the magnetization measured at several temperatures in the ordered and paramagnetic regions increases linearly with the magnetic field and its magnitude is similar for both field orientations, thus corroborating relatively weak magnetic anisotropy in the compound studied. No metamagnetic transition is seen for applied magnetic fields up to 5.5 T.

The presence of long-range magnetic order in UZn_{12} has been confirmed by preliminary muon spin relaxation experiments. The obtained zero-field μSR spectra were described using an exponential component in the muon depolarization function. Although no spontaneous frequency can be reliably extracted from the data, a fast depolarization rate of the order of $\lambda \sim$ 15-20 μs^{-1} was observed for $T \leq 5$ K (see figure 5). Such fast depolarization rates indicate the presence of strong internal fields at the muon stopping site(s), which can only be attributed to a magnetically ordered phase. The shape of the $\lambda(T)$ curve suggests that the depolarization rate scales with the ordered magnetic moment in UZn_{12}. In fact, in figure 5 we have included a fit to the data with the curve expected for the magnetic moments of a 3-dimensional Heisenberg antiferromagnet. Although the number of data points is very limited, there seems to be a good agreement between the data and the fit, indicating that the observed

depolarization rate scales with the magnetic moment of an ordered phase with the critical temperature of about 5 K.

3.3. Heat capacity

As displayed in figure 6, the specific heat of UZn_{12} measured in zero magnetic field exhibits a clear lambda-type anomaly near T_N = 5 K. Upon applying magnetic fields up to 10 T, directed within the *a*-*b* plane (see figure 7), the peak in *C(T)* shifts to lower temperatures, as expected for aniferrromagnets. The low-temperature zero-field heat capacity data are shown in the inset to figure 6 in the form *C/T(T)* versus T^2. From the linear portion of the plot between 10 and 17 K the electronic specific heat coefficient γ_p can be derived to be 203(3) mJ/(mol K^2). The ratio *C/T* is proportional to the temperature also below 3.7 K, and the $\gamma(0)$ value extracted from this region is as large as 714(2) mJ/(mol K^2). Though the magnitude of $\gamma(0)$ has to be verified in heat capacity studies extended to very low temperatures, far below T_N, the obtained estimates of the electronic contribution to the specific heat of UZn_{12} seem support the previously formulated hypothesis [8,9] that the compound can be classified as a heavy-fermion system.

3.4. Electrical transport properties

The temperature dependence of the electrical resistivity of UZn_{12}, measured with the current flowing in the hexagonal plane is presented in figure 8. The overall shape of $\rho(T)$ is characteristic of heavy-fermion compounds dominated by a single-ion Kondo effect at high temperatures and coherent Kondo scattering at low temperatures. From room temperature down to about 150 K, the resistivity changes with temperature in a logarithmic manner (see

the solid line in figure 8). At about 15 K, a maximum in ρ(*T*) is seen, which marks a crossover from incoherent to coherent Kondo regime. Below this temperature the resistivity decreases with decreasing temperature down to about 80 μΩcm at 2 K. This rather large value indicates significant residual scattering, mainly caused by the inherent atomic disorder, evidenced in the X-ray studies, but probably also due to significant disorder in the spin system that persists down to the lowest temperatures. As apparent from the inset to figure 8, hardly any singularity in ρ(*T*) occurs at the antiferromagnetic phase transition at T_N = 5 K. It seems likely that the expected change at T_N in the magnetic contribution to the resistivity is obscured by the much more effective scattering conduction electrons on structural and magnetic defects.

In an external magnetic field of 9 T, the magnetic phase transition in UZn_{12} becomes clearly evident (figure 9). For the field applied in the basal hexagonal plane a distinct hump in ρ(*T*) forms below 3 K, characteristic of scattering conduction electrons on "magnetic" Brillouin zone boundaries in antiferromagnets. This feature is accompanied with some change in slope of ρ(*T*) measured with *B* ∥ *c*-axis. The position of the onset of the antiferromagnetic state in 9 T corresponds well with the temperature of the peak in the specific heat that was taken in same field (compare figure 6). The observed direction-dependent response of the electrical transport on the applied field corroborates the afore-formulated hypothesis on the magnetic structure of UZn_{12} in which the magnetic moments are confined to the hexagonal *a*-*b* plane. In turn, the fairly distinct reduction of the resistivity by magnetic field supports the presumption on the significant magnetic character of the residual (defect) scattering in the compound in both the paramagnetic and antiferromagnetic states.

Figure 10 presents the isotherms of the magnetoresistance (MR = $\frac{\rho(B)-\rho(B=0)}{\rho(B=0)}\cdot 100\%$) measured on the UZn_{12} single crystal with the current flowing along

the crystallographic *a*-axis, and the magnetic field oriented either along the *c*-axis or perpendicular to it. For both orientations MR is negative at all temperatures studied. In the paramagnetic region, the isotherms show a typical Kondo-like dependence on the magnetic field, and in 9 T the magnitude of MR does not exceed 2.5 % for $B \perp c$ and only 0.6 % for $B \parallel c$. Below T_N = 5 K, the overall shape of the MR isotherms gradually changes towards a curvature characteristic of magnetically ordered systems. At 0.5 K, MR reaches a value of about 4 % for $B \perp c$ and 2.5 % for $B \parallel c$.

Given the Kondo character of UZn_{12}, the MR isotherms measured in the paramagnetic region can be analyzed in terms of the single-ion Kondo scaling relation $MR(B) = f[B/(T+T^*)]$, derived within the Bethe-Ansatz approach [14]. As is apparent from figure 11, for both configurations of the magnetic field the paramagnetic MR isotherms can be fairly well superimposed onto each other. The characteristic temperature T^*, which ensures the best overlap of the MR curves, are 6.8 K for $B \perp c$ and 29 K for $B \parallel c$. The difference in T^* reflects the orientation-dependent influence of the magnetic field on the electrical resistivity (cf. figure 9) and hints at important role played in UZn_{12} by spin fluctuations and single-ion anisotropy.

4. Conclusions

The high temperature solution growth technique was successfully employed to grow UZn_{12} single crystals with a stoichiometry close to the ideal 1:12 ratio. X-ray measurements confirm that this compound is isostructural with the hexagonal (P6/mmm) high-temperature form of the $SmZn_{12}$ compound. In this structure the uranium coordination environment and interatomic distances indicate weak *f-d* hybridization effects and therefore point to the possibility of appreciable uranium magnetic moments and magnetic ordering. Indeed, an

antiferromagnetic transition is observed at 5 K, with the uranium moments most probably confined within the *a*-*b* plane. This magnetic behaviour contrasts with the previous studies on polycrystalline samples having a higher degree of 4h zinc pairs substitution by uranium, where non transitions down to 0.4 K were observed, also suggesting an important role of disorder on the onset of magnetism. At high temperatures a modified Curie-Weiss law is followed, with μ_{eff} = ~2 μ_B/f.u. and θ = ~-40 K. No metamagnetic transitions were seen for applied magnetic fields up to 5.5 T. The γ_p and $\gamma(0)$ electronic specific heat coefficients are 202(3) mJ/(mol K-^{2}) and 714(2) mJ/(mol K^2), respectively, clearly pointing UZn_{12} as antiferromagnetic heavy-fermion system. Electrical transport curves are characteristic of a Kondo compound, with the magnetoresistance in the paramagnetic region being adjusted in terms of the single-ion Kondo scaling relation derived within the Bethe-Ansatz approach.

Acknowledgements

The authors would like to thank Dr. A. Amato and Dr. A. Schenck for assistance in the μSR experiments at the PSI. Part of the work was done in the frame of the Executive Programme of Scientific and Technological Cooperation between Portugal and Poland for the years 2009-2010. P.E. acknowledges the European Commission for a TMR grant. This work was partially supported by FCT, Portugal, under the contract nr. PTDC/QUI/65369/2006.

References

1- G.R. Stewart, Rev. Mod. Phys. **56**, 755 (1984).

2- N. Grewe, F. Steglich, in *Handbook of Physics and Chemistry of Rare Earths*, K.A. Gschneidner Jr., L. Eyring (Eds.), vol. 14, Elsevier, Amsterdam, 1991, p. 343.

3- P. Chiotti, J.T. Mason, J. Less-Common Metals **40**, 39 (1975).

4- C.L. Vold, D.T. Peterson, in Metallurgy and Ceramics, Research and Development, US-AEC report, 1961, p. 5.

5- H.R. Ott, H. Rudigier, P. Delsing, Z. Fisk, Phys. Rev. Lett. **52**, 1551 (1984).

6- J.O. Willis, Z. Fisk, R.M. Aikin, M.W. McElfresh, J.D. Thompson, E. Zirngiebl, J.A. O'Rourke, J.L. Smith, J. Appl. Phys. **61**, 4373 (1987).

7- J.T. Mason and P. Chiotti, Acta Cryst. **B27**, 1789 (1971).

8- Y. Nakazawa, M. Ishikawa, S. Noguchi and K. Okuda, Physica B **186-188**, 711 (1993).

9- Y. Nakazawa, M. Ishikawa, S. Noguchi and K. Okuda, J. Phys. Soc. Jpn. **62**, 3003 (1993).

10- A.C.T. North, D.C. Philips, F.S. Mathews, Acta Cryst. **A24**, 351 (1968).

11- J.O. Lundgren, Crystallographic Computer Programs, Report UUIC-B13-04-05 Inst. Chemistry, University of Uppsala, Sweden, 1982

12- B.K.Vainshtein, V.M.Fridkin and V.L.Indenbom, in "Modern Crystallography II, Structure of crystals", (M. Cardona, P. Fulde and H.-J. Queisser, Editors), Springer Series in Solid-State Sciences, Vol. 21, p. 71, Springer-Verlag, Berlin, 1982.

13- V. Sechovský and L. Havela, in Ferromagnetic Materials, edited by E. P. Wohlfarth and K. H. J. Buschow (North-Holland, Amsterdam, 1988), Vol. 4, p. 309.

14- P. Schlottmann, Phys. Rep. **181**, 1 (1989)

Table 1 - Parameters for the single crystal X-ray data collections

Crystal formula	UZn_{12}
Formula weight	1022.589 g/mol
Crystal system	Hexagonal
Space group	P6/mmm (No. 191)
Lattice parameters, Å a c	 8.9448(9) 8.8984(8)
Cell volume, $Å^3$	1849.7(5)
Z	3
Calculated density, g cm^{-3}	8.261
Linear absorption coefficient (mm^{-1})	12.70
Approximate crystal dimensions	0.1×0.1×0.1 mm^3
Radiation, wavelength	Mo K_α, 0.71073 Å
Monochromator	Graphite
Temperature	295 K
θ range; min. max. (deg)	1.5, 45
ω-2θ scan	$\Delta\omega = 0.80 + 0.35 \tan\theta$
Data set	$0 \le h \le 15$, $0 \le k \le 15$, $-15 \le l \le 15$
Number of measured reflections	3715
Number of unique reflections	756
Number of reflections with $I_o > 3\sigma(I_o)$	619
Number of refined parameters	37
R, wR2	0.0466, 0.0571
Goodness of fit	0.6
Structure solution program [11]	UPALS

Table 2 - Atomic coordinates (x, y, z), occupation factors (O.F.) and thermal parameters estimated in the UZn_{12} single-crystal X-ray diffraction structural refinement (the values with * were fixed).

Atom	X	Y	Z	O.F.	$B_{11}\times10^2$	$B_{22}\times10^2$	$B_{33}\times10^2$	$B_{12}\times10^2$	$B_{13}\times10^2$	$B_{23}\times10^2$
U_1 (*1a*)	0	0	0	1	0.20(1)	0.20(1)	0.0012*	0.10(1)	0	0
U_2 (*2d*)	1/3	2/3	1/2	0.98(1)	0.20(1)	0.20(1)	-0.01(1)	0.098(5)	0	0
U_3 (*2c*)	1/3	2/3	0	0.042(4)	0.0032*	0.0032*	0.2(2)	0.0016*	0	0
Zn_1 (*12o*)	0.1668(1)	0.3336(3)	0.2394(1)	0.98(1)	0.37(2)	0.40(2)	0.19(1)	0.20(1)	0.01(1)	0.01(1)
Zn_2 (*6j*)	0.3562(3)	0	0	0.96(1)	0.59(3)	1.25(5)	0.09(2)	0.63(2)	0	0
Zn_3 (*6k*)	0.2932(2)	0	1/2	0.97(1)	0.50(2)	0.22(3)	0.06(1)	0.11(1)	0	0
Zn_4 (*6i*)	1/2	0	0.2784(1)	0.98(1)	0.23(2)	0.24(3)	0.24(1)	0.12(1)	0	0
Zn_5 (*2e*)	0	0	0.3531(3)	0.96(2)	0.44(4)	0.44(4)	0.04(3)	0.22(2)	0	0
Zn_6 (*4h*)	1/3	2/3	0.1453(2)	0.958(4)	0.43(2)	0.43(2)	0.20(2)	0.22(1)	0	0

Table 3 - Interatomic distances (d), nearest-neighbours (NN) and coordination (CN) numbers.

atom	d (Å)	NN	CN	atom	d (Å)	NN	CN	atom	d (Å)	NN	CN
U_1 - Zn_5	3.1420	2		Zn_1 - Zn_1	2.5842	2		Zn_4 - Zn_1	2.6043	4	
- Zn_2	3.1861	6	20	- Zn_4	2.6043	2		- Zn_3	2.7037	2	
- Zn_1	3.3491	12		- Zn_2	2.6658	2		- Zn_2	2.7913	2	14
				- Zn_3	2.6823	2		- Zn_6	2.8408	2	
U_2 - Zn_6	3.1563	2		- Zn_6	2.7126	1	13	- U_2	3.2490	2	
- Zn_3	3.1764	6		- Zn_5	2.7752	1		- U_3	3.5783	2	
- Zn_4	3.2490	6	20	- U_3	3.3459	1					
- Zn_1	3.4691	6		- U_1	3.3491	1		Zn_5 - Zn_5	2.6143	1	
				- U_2	3.4691	1		- Zn_1	2.7752	6	
U_3 - Zn_6	1.2929	2						- Zn_3	2.9303	6	14
- Zn_2	2.8848	6		Zn_2 - Zn_2	2.5725	1		- U_1	3.1420	1	
- Zn_1	3.3459	6	20	- Zn_1	2.6658	4					
- Zn_4	3.5783	6		- Zn_4	2.7913	2		Zn_6 - U_3	1.2929	1	
				- Zn_6	3.1612	4	16	- Zn_6	2.5859	1	
				- Zn_2	3.1862	2		- Zn_1	2.7125	3	15
				- U_3	2.8848	2		- Zn_4	2.8408	3	
				- U_1	3.1861	1		- Zn_2	3.1612	6	
								- U_2	3.1563	1	
				Zn_3 - Zn_3	2.6226	6					
				- Zn_1	2.6823	4					
				- Zn_4	2.7037	2	16				
				- Zn_5	2.9303	2					
				- U_2	3.1764	2					

Figure captions

Fig. 1 - UZn_{12} crystal structure.

Fig. 2 –Coordination polyedra of the different U sites.

Fig. 3 - Temperature dependence of the inverse susceptibility of UZn_{12} for a field of 5 T applied along the *a* axis (closed symbols) and the *c* axis (open symbols). The inset shows an enlarged view of the low temperature magnetic susceptibility.

Fig. 4 - Magnetization versus field of UZn_{12} along the *a* axis (4a) and the *c* axis (4b) between 2 K and 200 K.

Fig. 5 - Temperature dependence of the zero-field μSR depolarization rate in polycrystalline UZn_{12}. The line is a fit with a 3D Heisenberg antiferromagnet model.

Fig. 6 - Heat capacity C versus temperature of UZn_{12}. The inset shows the heat capacity C/T versus T^2.

Fig. 7 - Heat capacity C versus temperature of UZn_{12} in magnetic fields up to 10 T for B perpendicular to the *c* axis.

Fig. 8 - Temperature dependence of the electrical resistivity of UZn_{12} for i//*a* axis. The inset shows an enlarged view of the low temperature region.

Fig. 9- Resistivity versus temperature of UZn_{12} under 0 T and 9 T magnetic fields applied parallel to the (*ab*) plane and along the *c* axis.

Fig 10- Magnetoresistivity of UZn_{12} shown for various temperatures, $0.5\ K \leq T \leq 25\ K$, with fields along the (*ab*) plane and current parallel to the *a* axis (10a) and with fields along the *c* axis and current parallel to the *a* axis (10b).

Fig. 11- Kondo scaling of the magnetoresistance of UZn_{12} measured with fields along the (*ab*) plane and current parallel to the *a* axis (11a) and with fields along the *c* axis and current parallel to the *a* axis (11b).

Fig 1

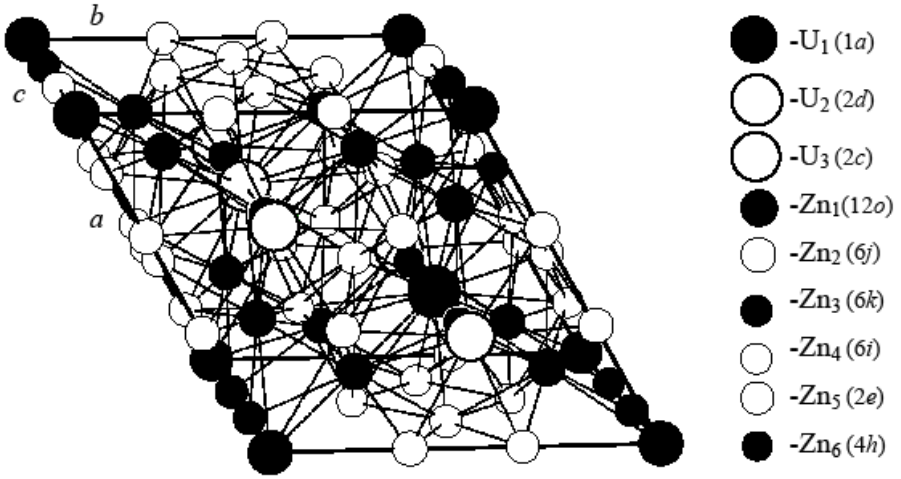

Fig 2

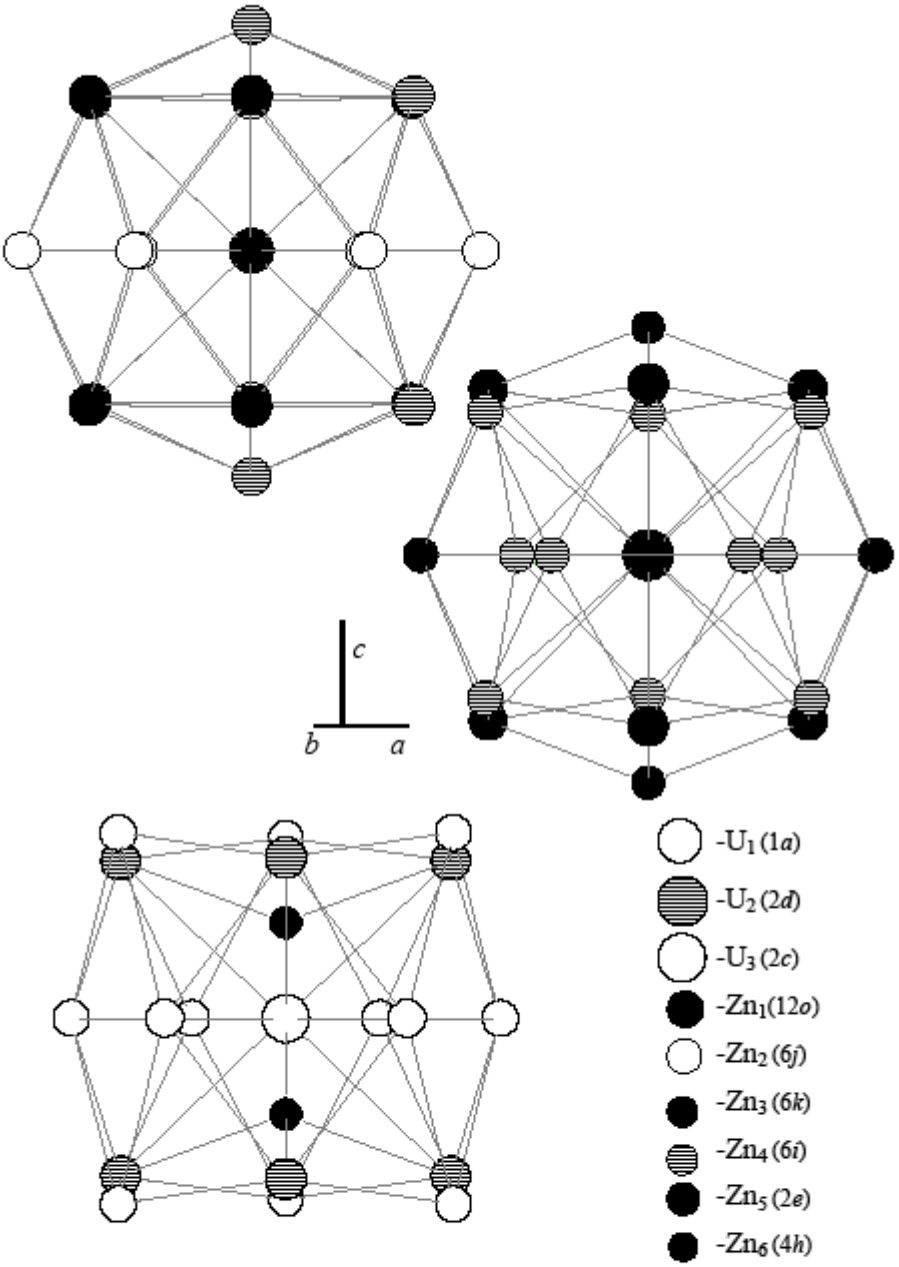

Fig 3

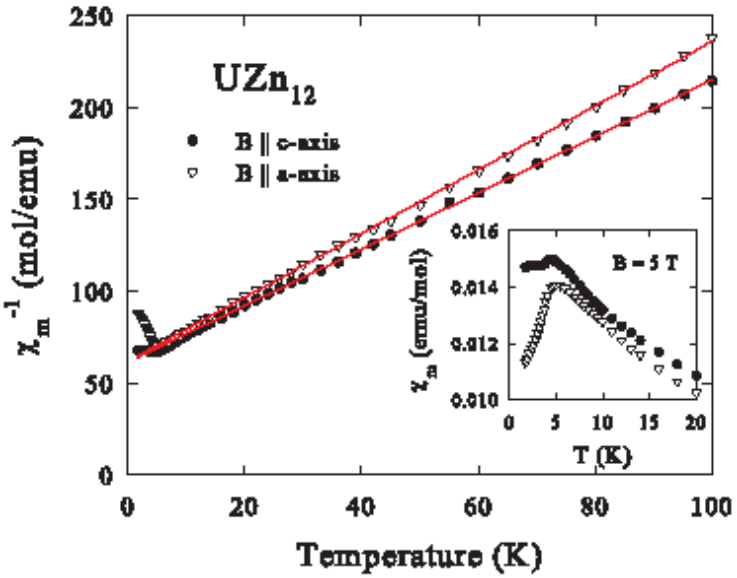
UZn12
B || c-axis
B || a-axis
B = 5 T
χm (emu/mol)
T (K)
χm-1 (mol/emu)
Temperature (K)

Fig 4

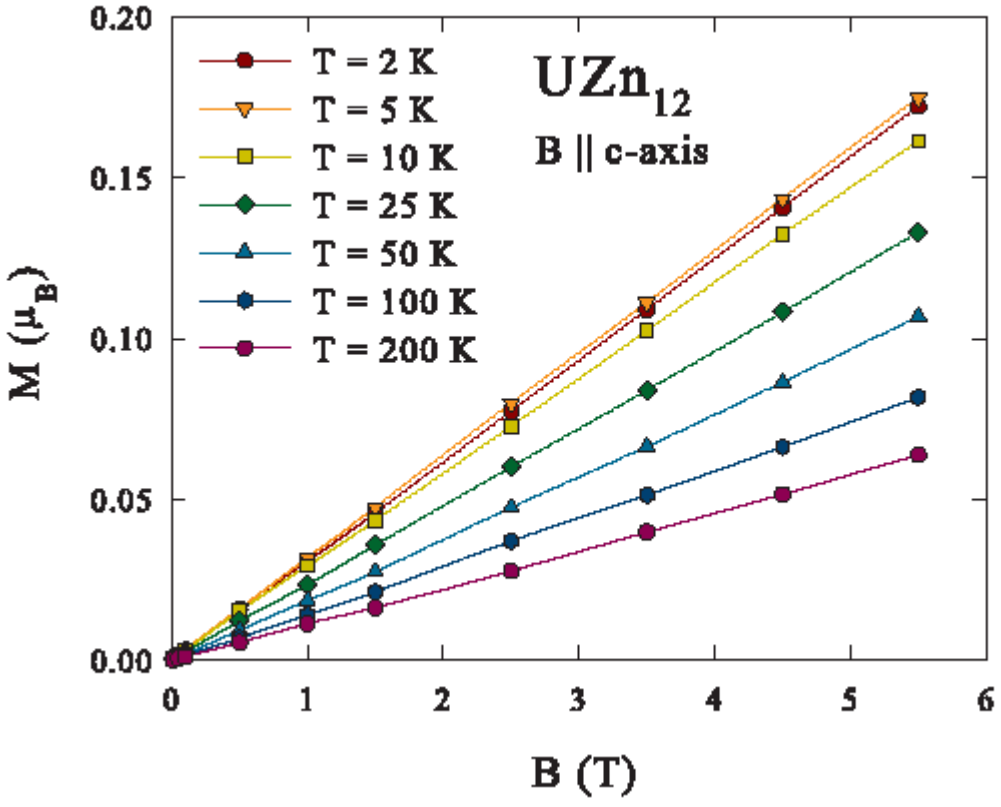
0.20
0.15
0.10
0.05
0.00
M (μ_B)
0
1
2
3
4
5
6
B (T)
T = 2 K
T = 5 K
T = 10 K
T = 25 K
T = 50 K
T = 100 K
T = 200 K
UZn12
B || c-axis

Fig 5

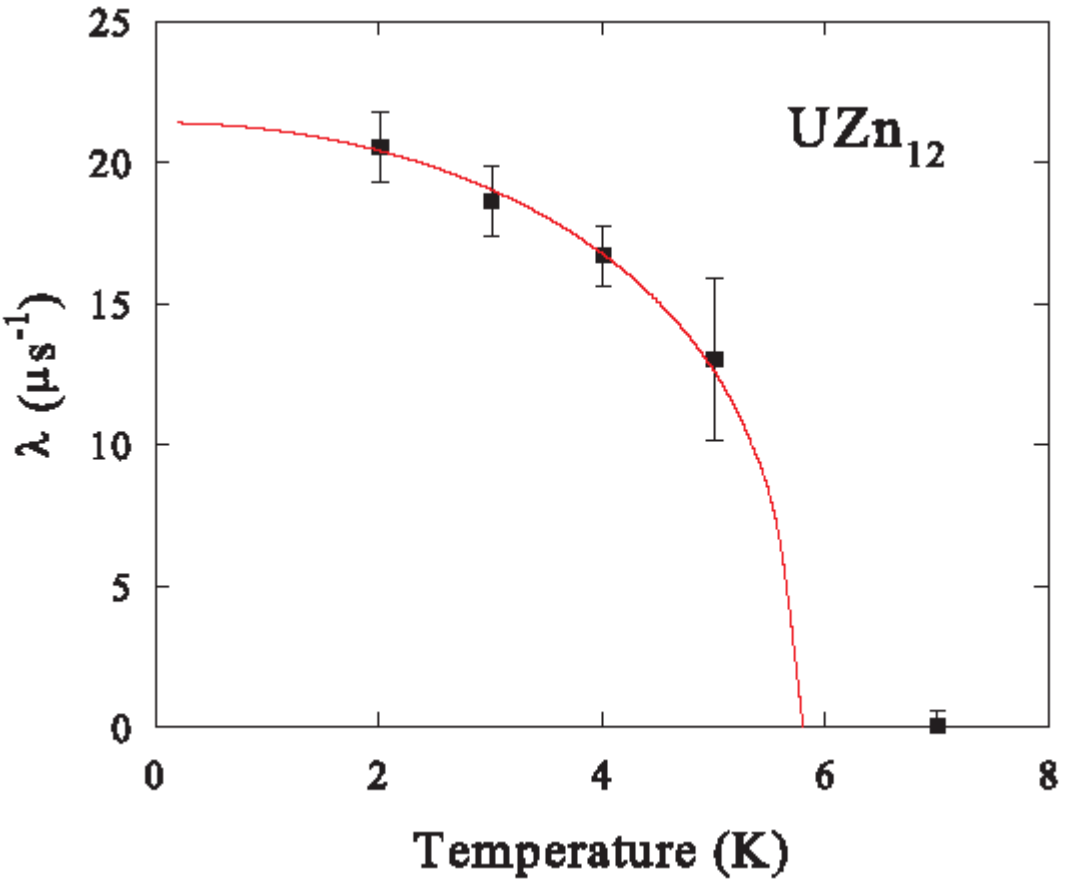

Fig 6

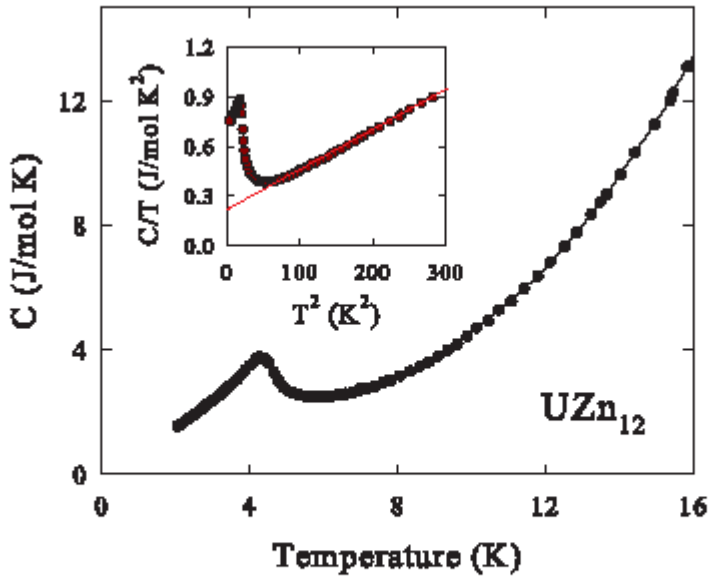
C (J/mol K)
Temperature (K)
UZn12
C/T (J/mol K2)
T2 (K2)
0
4
8
12
16
0.0
0.3
0.6
0.9
1.2
100
200
300

Fig 7

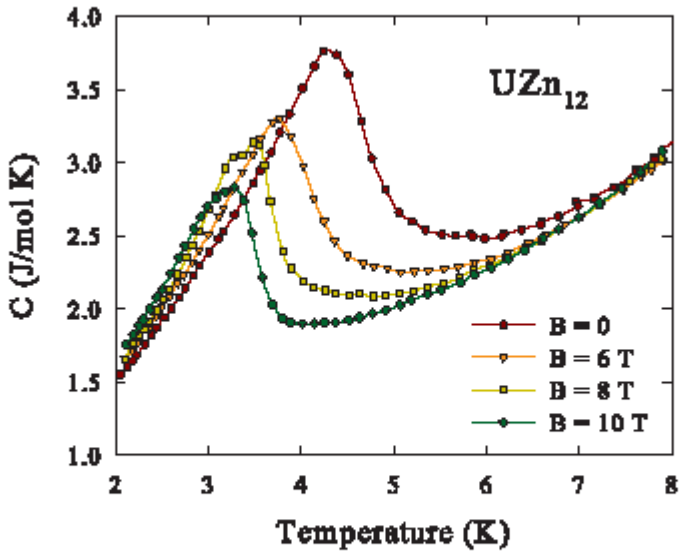
UZn12
C (J/mol K)
Temperature (K)
B = 0
B = 6 T
B = 8 T
B = 10 T
4.0
3.5
3.0
2.5
2.0
1.5
1.0
2
3
4
5
6
7
8

Fig. 8

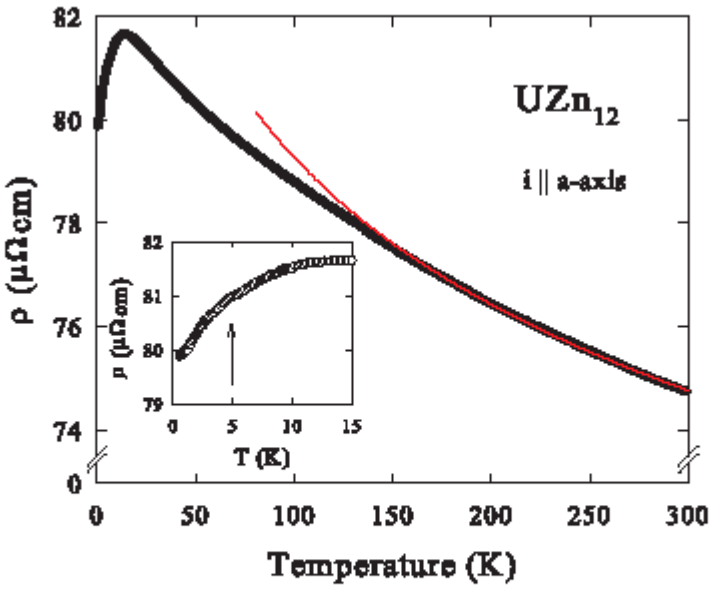
UZn12
i || a-axis
ρ (μΩcm)
Temperature (K)
T (K)
82
80
78
76
74
0
50
100
150
200
250
300
81
79
5
10
15

Fig. 9

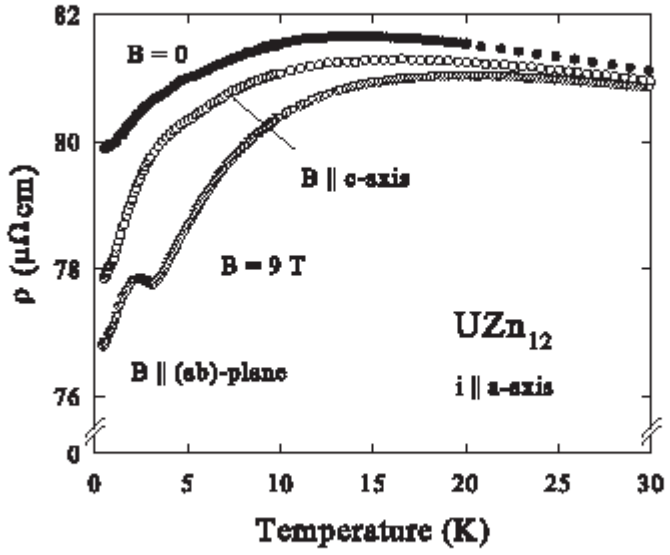
82
80
78
76
0
ρ (μΩcm)
B = 0
B ∥ c-axis
B = 9 T
B ∥ (ab)-plane
UZn12
i ∥ a-axis
0
5
10
15
20
25
30
Temperature (K)

Fig. 10

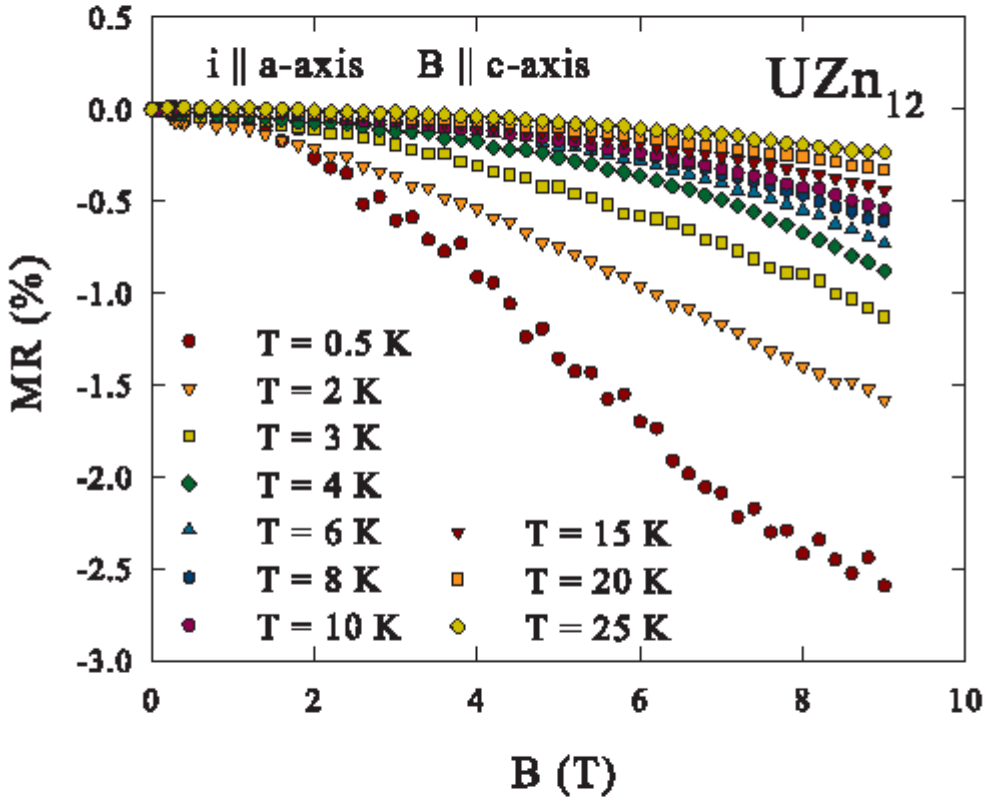
i ∥ a-axis
B ∥ c-axis
UZn12
T = 0.5 K
T = 2 K
T = 3 K
T = 4 K
T = 6 K
T = 8 K
T = 10 K
T = 15 K
T = 20 K
T = 25 K
MR (%)
B (T)
0.5
0.0
-0.5
-1.0
-1.5
-2.0
-2.5
-3.0
0
2
4
6
8
10

Fig. 11

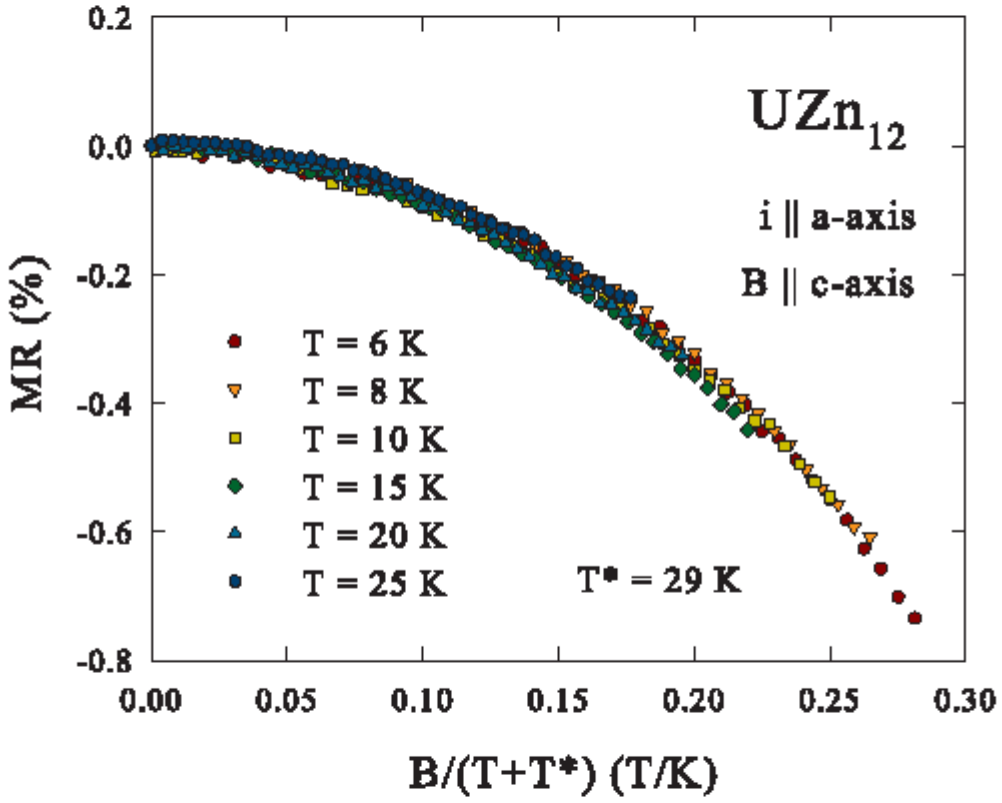
UZn12
i || a-axis
B || c-axis
T = 6 K
T = 8 K
T = 10 K
T = 15 K
T = 20 K
T = 25 K
T* = 29 K
MR (%)
B/(T+T*) (T/K)
0.2
0.0
-0.2
-0.4
-0.6
-0.8
0.00
0.05
0.10
0.15
0.20
0.25
0.30